International Journal of Pharmacology

Int. J. Pharmacol. **2025**; 21(5): 44207
https://doi.org/10.31083/IJP44207

Research Article

Effects of Bioactive Glass Carrier-Loaded Sacubitril/Valsartan Sodium Tablets on Cardiomyocytes From Rats With Chronic Heart Failure

Fan Jia[1], Yi Ma[1], Xuebin Geng[1], Li Li[1,*]

[1]Department of Cardiovascular Medicine, Tangshan Workers' Hospital, 063000 Tangshan, Hebei, China
*Correspondence: lilitshn@yeah.net (Li Li)
Academic Editor: Mehmet Ozaslan
Published: 23 September 2025

Abstract

Background and Objective: Sacubitril/valsartan sodium tablets (SVSTs) represent a therapeutic option for chronic heart failure (CHF), functioning by inhibiting angiotensin II receptors and neprilysin. Thus, this study aimed to develop mesoporous nano-bioactive glass (MNBG)-loaded SVSTs to enhance the bioavailability of SVSTs and investigate the treatment effects on myocardial cell autophagy and apoptosis in rats with CHF. **Materials and Methods**: The MNBG-loaded SVSTs were prepared and tested in normal Sprague-Dawley rats (Ctrl group) and CHF models created through abdominal aortic ligation. The rats were divided into CHF, SVST, and SVST/MNBG groups (15 rats each). Cardiac function, myocardial tissue pathology, and the levels of reactive oxygen species (ROS), nitric oxide (NO), creatine kinase-MB (CK-MB), N-terminal pro-B-type natriuretic peptide (NT-proBNP), apoptosis-related proteins (Bcl-2 and Bax), and autophagy-related proteins (Atg5, beclin1, p62, and LC3II/I) were assessed. Statistical analysis was performed using SPSS 26.0 via one-way analysis of variance (ANOVA), *t*-test, and χ^2 test ($p < 0.05$). **Results**: The CHF group demonstrated reduced cardiac function with increased ROS, CK-MB, NT-proBNP levels, and decreased NO levels, along with altered protein expression (decreased Bcl-2, Atg5, beclin1, p62, and increased Bax, LC3II/I). The SVST and SVST/MNBG groups presented improved cardiac function, reduced ROS, CK-MB, and NT-proBNP levels, increased NO, and favorable protein expression changes. The SVST/MNBG group showed superior improvements compared to the SVST group ($p < 0.05$). **Conclusion**: Loading MNBG with SVSTs can improve cardiac function in CHF models and exert the effects of SVSTs by influencing cardiomyocytes to promote autophagy–apoptosis. These findings provide preliminary evidence for identifying potential candidates to treat heart failure.

Keywords: mesoporous nano-bioactive glass; sacubitril/valsartan sodium tablets; heart failure; autophagy; cardiomyocyte apoptosis; myocardial tissue pathology

1. Introduction

Heart failure (HF) is a pathological state in which the heart cannot pump blood with sufficient force [1,2]. During the progression of HF, cellular autophagy plays a crucial role by influencing cellular homeostasis, removing damaged substances and regulating energy metabolism [3]. Apoptosis, a regulated form of cell death, is closely related to the loss of cardiomyocytes and myocardial remodeling in HF [4].

Sacubitril/valsartan sodium tablets (SVST) are a combination formulation consisting of sacubitril and valsartan [5]. This combination works by blocking angiotensin receptors and inhibiting neprilysin, which reduces vasoconstriction, thereby decreasing the heart's afterload and improving cardiac function [6]. Long-term use of SVST can inhibit myocardial hypertrophy, reduce myocardial fibrosis, improve myocardial remodeling and delay the progression of HF [7]. Clinical trials showed that SVST greatly reduce hospitalization rates and mortality in patients with chronic HF (CHF), thereby improving patient outcomes [8]. However, systemic drug delivery systems often face issues such as low local drug concentration and suboptimal therapeutic effects. Therefore, selecting ideal drug delivery materials is crucial for enhancing treatment efficacy. Bioactive glass (BG) is a novel biomaterial known for its excellent biocompatibility and bioactivity, without causing notable immune responses or toxic effects [9]. Clinically, BG is utilized in various forms including powders, granules, granule/fiber composites, coatings, or implants. It can be applied to patients through surgical implantation or direct coating on damaged tissue surfaces to achieve therapeutic effects [10,11]. The BG can upregulate the expression level of genes related to soft tissue repair, such as vascular endothelial growth factor. The BG is utilized in cardiovascular research for repair and regeneration applications [12]. Its properties of promoting cell regeneration and suppressing inflammatory responses make it a promising candidate for potential strategies in the treatment of HF.

Therefore, this work investigated the effects of SVST-loaded mesoporous nano-BG (MNBG) on myocardial cell autophagy and apoptosis in CHF rats. By examining the role of BG in HF, this research sought to provide new insights and strategies for the treatment of HF, enhance myocardial cell protection and promote functional recovery, ultimately improving patient outcomes.

2. Materials and Methods

2.1 Study Area

The research was performed in Tangshan Workers' Hospital from December, 2022 to January, 2024.

2.2 Fabrication of Drug-loaded Mesoporous BG Microspheres

Mesoporous BG microspheres were prepared to adopt the sol-gel methodology [13]. A mixture of tri-block copolymer P123 (4.0 g), triethyl phosphate (0.73 g), 0.5 mol/L hydrochloric acid (1.0 g), ethanol (60 g), tetraethyl orthosilicate (6.7 g) and calcium nitrate (1.4 g) was stirred continuously at 25 °C for 24 hrs. They were calcined at 700 °C for 5 hrs to obtain mesoporous BG. A 1 g/L suspension of the mesoporous BG was prepared and mixed with a 1 g/L aqueous solution of SVST. The mixture was shaken horizontally at 24 °C for 24 hrs in the dark, then centrifuged at 3000 rpm for 5 min to remove supernatant. Precipitate was rinsed thrice with deionized water, dried at 37 °C using a WH-A-5 electric hot air-drying oven (WHA5, Nanjing Wohuan Technology Co., Ltd., Nanjing, China) and ground to obtain the mesoporous BG microspheres loaded with SVST (SVST/MNBG).

2.3 Characterization of Drug-loaded Mesoporous BG Microspheres

The microscopic morphology and particle size of SVST/MNBG were examined using a ZEM20 scanning electron microscope (ZEM 20, Anhui ZEPTOOLS Technology Co., Ltd., Tongling, China). Nitrogen adsorption/desorption experiments were conducted at liquid nitrogen temperature using an ASAP2010 analyzer (Micromeritics Instrument Corp., Norcross, GA, USA). Pore distribution was computed using Barrett-Joyner-Halenda (BJH) methodology [13].

2.4 Assessment of Drug Release Capacity of Drug-loaded Mesoporous BG Microspheres

The drug release profile of SVST/MNBG was assessed using a UV5 Nano UV-Vis spectrophotometer (Mettler Toledo, Columbus, OH, USA). Fifty milligrams of SVST/MNBG particles were placed in a dialysis bag with a molecular weight cutoff of 3500 and diluted with 5 mL of phosphate-buffered saline (PBS). The dialysis bag was immersed in PBS (45 mL, pH = 7.4), sealed and incubated at 37 °C with shaking. Samples were collected at 3, 6, 12, 24, 72, 168, 336 and 504 hrs. Absorbance was measured at 350 nm to determine the content of sacubitril/valsartan sodium, using a standard curve for calculation. After each sampling, an equal volume of PBS was applied to maintain the consistency of liquid volume in the system.

2.5 Animals and Grouping

Sixty specific pathogen-free Sprague Dawley rats (male, 200–250 g; Chengdu Dashuo Experimental Animal Co., Ltd., Chengdu, China) were selected for this experiment. Rats were kept at 23 ± 2 °C, relative humidity of 50 ± 5%, low light with a 12 hrs light/dark cycle, well-ventilated and noise levels below 80 dB for one week before modeling. Fasting lasted for 8 hrs before the procedure and rats can have water.

Sixty rats were randomly allocated into four groups: Ctrl group, CHF group, SVST group and SVST/MNBG group (each with 15 rats). The Ctrl group received no treatment. The CHF, SVST and SVST/MNBG groups first underwent CHF modeling. For this, rats were anesthetized with a 40 mg/kg intraperitoneal injection of sodium pentobarbital (Suicheng Pharmaceutical Co., Ltd., Zhengzhou, China) and a midline abdominal incision 2.5 cm below the xiphoid process was made. The abdominal cavity was exposed and the abdominal aorta was isolated and ligated to achieve a 50% circumferential constriction. After 4 weeks of modeling, a cardiac ultrasound was performed, with a left ventricular ejection fraction (LVEF) of <45% considered as the criterion for successful modeling [14]. The SVST group received a continuous gavage of 10 mg/kg/day SVST dissolved in water for 6 weeks post-surgery. The SVST/MNBG group received a continuous gavage of 10 mg/kg/day MNBG suspension for 6 weeks post-surgery.

2.6 Ethical Consideration

All stages of the study were carried out according to ethical principles and accepted by the Ethics Committee for Animal Experiments.

2.7 Color Doppler Ultrasound Detection

Four weeks after cessation of treatment, rats were anesthetized by intraperitoneal injection of sodium pentobarbital (40 mg/kg). Upon achieving anesthesia, they were secured in a supine position for cardiac function assessment. Cardiac function parameters, including LV end-diastolic dimension (LVEDD), LVE-systolic dimension (LVESD), LVEF, LV fractional shortening (LVFS), LV posterior wall end-diastolic thickness (LVPWD) and LV posterior wall end-systolic thickness (LVPWS), were measured via DW-T5 color Doppler ultrasound diagnostic system (Dawei Medical Co., Ltd., Shenzhen, China). Each parameter was recorded in triplicate for statistical analysis.

2.8 ELISA

Following the completion of ultrasound examinations, all rats were euthanized via intraperitoneal injection of sodium pentobarbital (150 mg/kg) in accordance with experimental animal ethics guidelines and the chemical euthanasia standards recommended by the *American Veterinary Medical Association (AVMA) Guidelines for the Euthanasia of Animals (2020 Edition)* [15]. After confirming deep anesthesia and complete cessation of vital signs, the hearts were excised. One-third of the myocardial tissue was homogenized using a high-throughput vibration

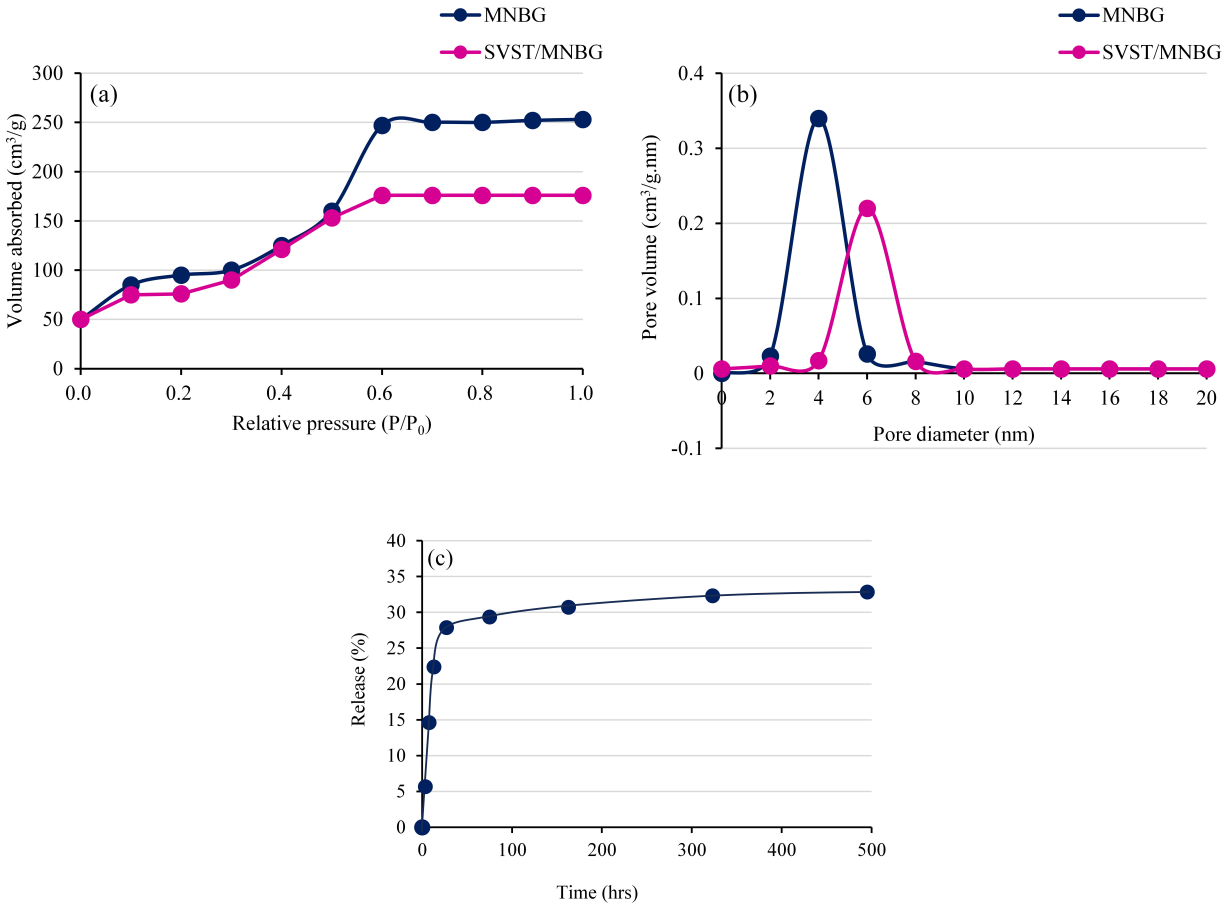

Fig. 1. Characterization of MNBG. (a) Nitrogen adsorption/desorption isotherms, (b) Pore size distribution curve and (c) Drug release profile over time. SVST, Sacubitril/valsartan tablets; MNBG, Mesoporous nano-bioactive glass.

grinder (Model HG100, Zhiheng Scientific Instruments Co., Ltd., Shanghai, China). The homogenized tissue was centrifuged at 2500 rpm for 10 min and the supernatant was collected. The expression levels of Reactive Oxygen Species (ROS), nitric oxide (NO), Creatine Kinase-MB isoenzyme (CK-MB) and NT-proBNP in the myocardial tissue were measured via kits (ROS kit, Cat# E004-1-1; NO kit, Cat# A012-1-2; CK-MB kit, Cat# H197; NT-proBNP kit, Cat# H255, Shanghai Westang Biotechnology Co., Ltd., Shanghai, China).

2.9 Hematoxylin and Eosin (H&E) Staining

One-third of the myocardial tissue was processed for routine dehydration and sectioned into 4 µm thick paraffin slices. The slices were dewaxed by baking at 60 °C for 20 min, followed by immersion in Xylene I and Xylene II for 5 min each and sequentially rinsed with graded alcohol solutions from high to low concentrations. According to the instructions of the H&E staining kit (Cat# G1120, Beijing Solarbio Science & Technology Co., Ltd., Beijing, China), the tissue sections were stained with H&E for 10 min each, rinsed with tap water for 10 min and then rinsed with distilled water before dehydration with 95% ethanol. After clearing with xylene, sections were mounted with neutral gum and examined under a BX53 optical microscope (BX53, Olympus Corp., Tokyo, Japan) to visualize pathological changes.

2.10 Western Blotting

One-third of the myocardial tissue was taken and 100 µL of Radio-immunoprecipitation assay (Cat# R0278, Sigma-Aldrich, St. Louis, MO, USA) buffer was applied to thoroughly lyse the tissue and extract the total protein. The extract was then heated to 100 °C in a DK-S12 water bath (Model DK-S12, Shanghai Jingqi Instrument Co., Ltd., Shanghai, China) to denature the proteins. The bicinchoninic acid kit (Cat# BCA1, Sigma-Aldrich, St. Louis, MO, USA) determined protein concentrations. Protein (30 µg) was loaded for electrophoresis, separated and transferred to a membrane, which was subsequently blocked at 25 °C for 2 hrs. It was incubated overnight at 4 °C with primary antibodies against Bcl-2, Bax, Atg5, Beclin1, p62, LC3-I, LC3-II and GAPDH (all diluted 1:2000; Cat# ab182858, ab32503, ab109490, ab62557, ab109012, ab192890, ab232940, ab8245; Abcam, Cambridge, MA, USA). After the membranes were washed, the secondary

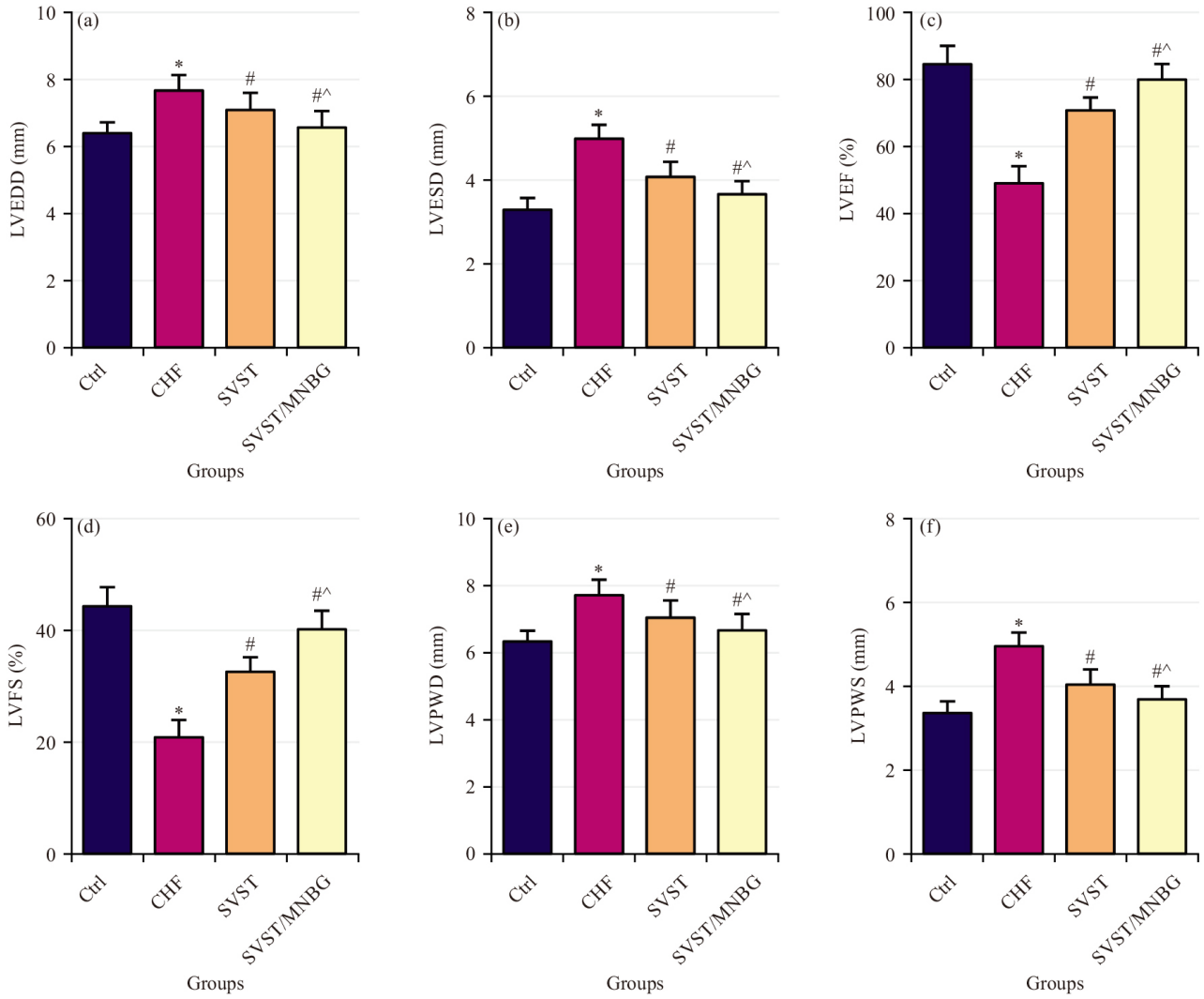

Fig. 2. Cardiac function indicators of rats in each group. (a) LVEDD, (b) LVESD, (c) LVEF, (d) LVFS, (e) LVPWD and (f) LVPWS. LVEDD, Cardiac function parameters; including LV end-diastolic dimension; LVESD, LVE-systolic dimension; LVEF, Left Ventricular Ejection Fraction; LVFS, LV fractional shortening; LVPWD, LV posterior wall enddiastolic thickness; LVPWS, LV posterior wall end-systolic thickness, *$p < 0.05$ vs Ctrl group, $^{\#}p < 0.05$ vs CHF group and $^{\wedge}p < 0.05$ vs SVST group.

antibody, horseradish peroxidase-conjugated anti-mouse IgG-HRP (diluted 1:5000; Cat# ab6721, Abcam, Cambridge, MA, USA), was added and incubated at 25 °C for 2 h. Following additional washes, an enhanced chemiluminescence reagent (Cat# E2529, Sigma-Aldrich, St. Louis, MO, USA) was utilized for detection and imaging was conducted with a WD-9413A gel imaging system (Model WD-9413A, Beijing Liuyi Biotechnology Co., Ltd., Beijing, China). The GAPDH was utilized as a loading control and the relative optical density of the target proteins was calculated employing Image-Pro Plus 6.0 (Media Cybernetics Inc., Rockville, MD, USA) [13].

2.11 Statistical Analysis

Data were processed using SPSS 26.0 (IBM, Armonk, NY, USA). Quantitative data (Mean $\pm$ Standard Deviation ($\bar{\chi} \pm s$)) were compared among groups utilizing One-way ANOVA, with between-group comparisons conducted via *t*-test. Categorical data (frequencies or rates) were compared between groups via χ^2 test. The $p < 0.05$ implied statistical significance.

3. Results

3.1 Characterization and Drug Release Analysis of MNBG

First, nitrogen adsorption/desorption isotherm analysis were conducted for MNBG and SVST/MNBG (Fig. 1a). Both samples exhibited type IV isotherms, indicative of typical mesoporous solid adsorption. Next, pore size distribution analysis was performed for MNBG and SVST/MNBG (Fig. 1b), revealing a single characteristic peak for both samples, located at 4.1 and 6.0 nm, respectively. Finally, the *in vitro* drug release profile of

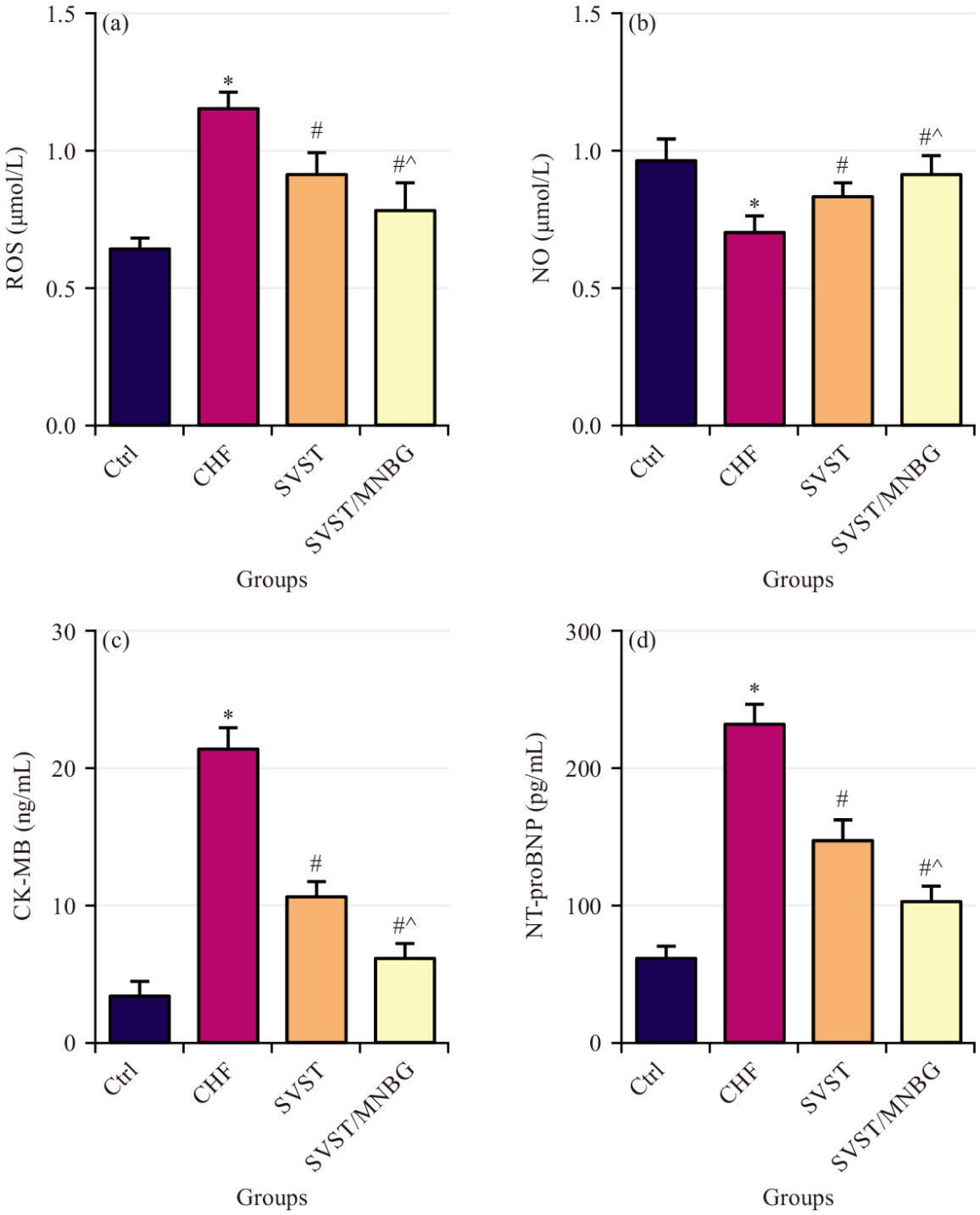

Fig. 3. Cytokine levels in rat myocardial tissue. (a) ROS, (b) NO, (c) CKMB and (d) NT-proBNP. ROS, Reactive Oxygen Species; NO, Nitric oxide; CK-MB, Creatine Kinase-MB isoenzyme; NT-proBNP, N-terminal pro-B-type natriuretic peptide, *$p < 0.05$ vs Ctrl group, $^{\#}p < 0.05$ vs CHF group and $^{\wedge}p < 0.05$ vs SVST group.

SVST/MNBG was analyzed (Fig. 1c). It was observed that a burst release occurred within the first 0–12 hrs, followed by a stable drug release concentration of approximately 45 mg/L from 24 to 504 hrs, with a drug loading capacity of 33%.

3.2 Cardiac Function Evaluation

Comparisons were made of cardiac function parameters among the different groups, including LVEDD, LVESD, LVEF, LVFS, LVPWD and LVPWS (Fig. 2a–f). The CHF group exhibited drastic increases in LVEDD, LVESD, LVPWD and LVPWS versus Ctrl group, along

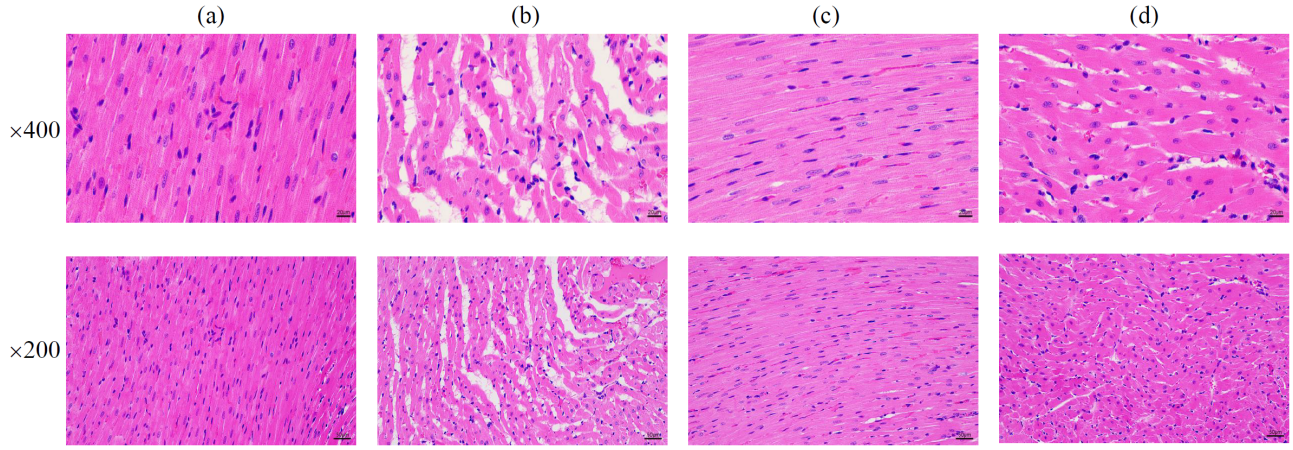

Fig. 4. Pathological morphology of myocardial tissue in each group of rats (×200, ×400). (a) Ctrl group, (b) CHF group, (c) SVST group and (d) SVST/MNBG group. CHF, Chronic heart failure; SVST, Sacubitril/valsartan tablets; MNBG, Mesoporous nano-bioactive glass. Scale bar = 20 µm, 50 µm.

with great declines in LVEF and LVFS ($p < 0.05$). In comparison to the CHF group, SVST and SVST/MNBG groups showed prominent reductions in LVEDD, LVESD, LVPWD and LVPWS and substantial increases in LVEF and LVFS ($p < 0.05$). Furthermore, relative to the SVST group, the SVST/MNBG group demonstrated notably lower LVEDD, LVESD, LVPWD and LVPWS and higher LVEF and LVFS ($p < 0.05$).

3.3 Cytokine Levels Related to Myocardial Tissue

Comparisons were made of ROS (Fig. 3a), NO (Fig. 3b), CK-MB (Fig. 3c) and NT-proBNP (Fig. 3d) in myocardial tissue across various groups. The CHF group exhibited greatly increased ROS, CK-MB and NT-proBNP and a markedly decreased NO versus Ctrl group ($p < 0.05$). The SVST and SVST/MNBG groups showed notable reductions in ROS, CK-MB and NT-proBNP and increased NO versus the CHF group ($p < 0.05$). Additionally, relative to the SVST group, SVST/MNBG group demonstrated notably lower ROS, CK-MB and NT-proBNP and a considerably higher NO ($p < 0.05$).

3.4 Pathological Evaluation of Myocardial Tissue

In Fig. 4a–d, Ctrl group exhibited clear myocardial tissue structure with orderly fiber arrangement and well-defined, uniform-sized nuclei. In contrast, the CHF group showed blurred myocardial tissue structure with disorganized fiber arrangement, including fragmentation and nuclei appeared fragmented and incomplete. Myocardial cell hypertrophy and swelling were evident. Relative to the CHF group, SVST and SVST/MNBG groups displayed relatively clearer myocardial tissue structures and uniform nuclei sizes. Nevertheless, a small amount of fiber fragmentation and cytoplasmic vacuolation in myocardial cells was still observed.

3.5 Cardiomyocyte Apoptosis

Comparisons were made of the relative expression levels of Bcl-2 and Bax (Fig. 5a–c) in myocardial tissue across different groups. The CHF group exhibited a notable decrease in the relative expression level of Bcl-2 and a marked elevation in the relative expression level of Bax ($p < 0.05$). The SVST and SVST/MNBG groups showed markedly higher relative expression levels of Bcl-2 and greatly lower expression levels of Bax ($p < 0.05$). Additionally, relative to the SVST group, the SVST/MNBG group demonstrated a substantially greater increase in Bcl-2 expression level and a more pronounced decrease in Bax expression level ($p < 0.05$).

3.6 Myocardial Cell Autophagy

Comparisons were made of the relative expression levels of autophagy-related proteins Atg5, Beclin1, p62 and LC3 (Fig. 6a–e) in myocardial tissue across various groups. Relative to Ctrl group, CHF group showed notably reduced relative expression levels of Atg5, Beclin1 and p62, along with a marked increase in the LC3II/I relative expression level ($p < 0.05$). The SVST and SVST/MNBG groups exhibited markedly higher relative expression levels of Atg5, Beclin1 and p62 and a greatly lower LC3II/I ratio ($p < 0.05$). Additionally, SVST/MNBG group demonstrated notably higher relative expression levels of Atg5, Beclin1 and p62 and a greatly lower LC3II/I relative expression level ($p < 0.05$).

4. Discussion

The SVST/MNBG greatly improved cardiac function in CHF model rats, demonstrating superior efficacy versus SVST alone. Relative to traditional drug delivery methods, nanocarrier systems offer advantages such as enhanced solubility of poorly soluble drugs, maintenance of drug bioac-

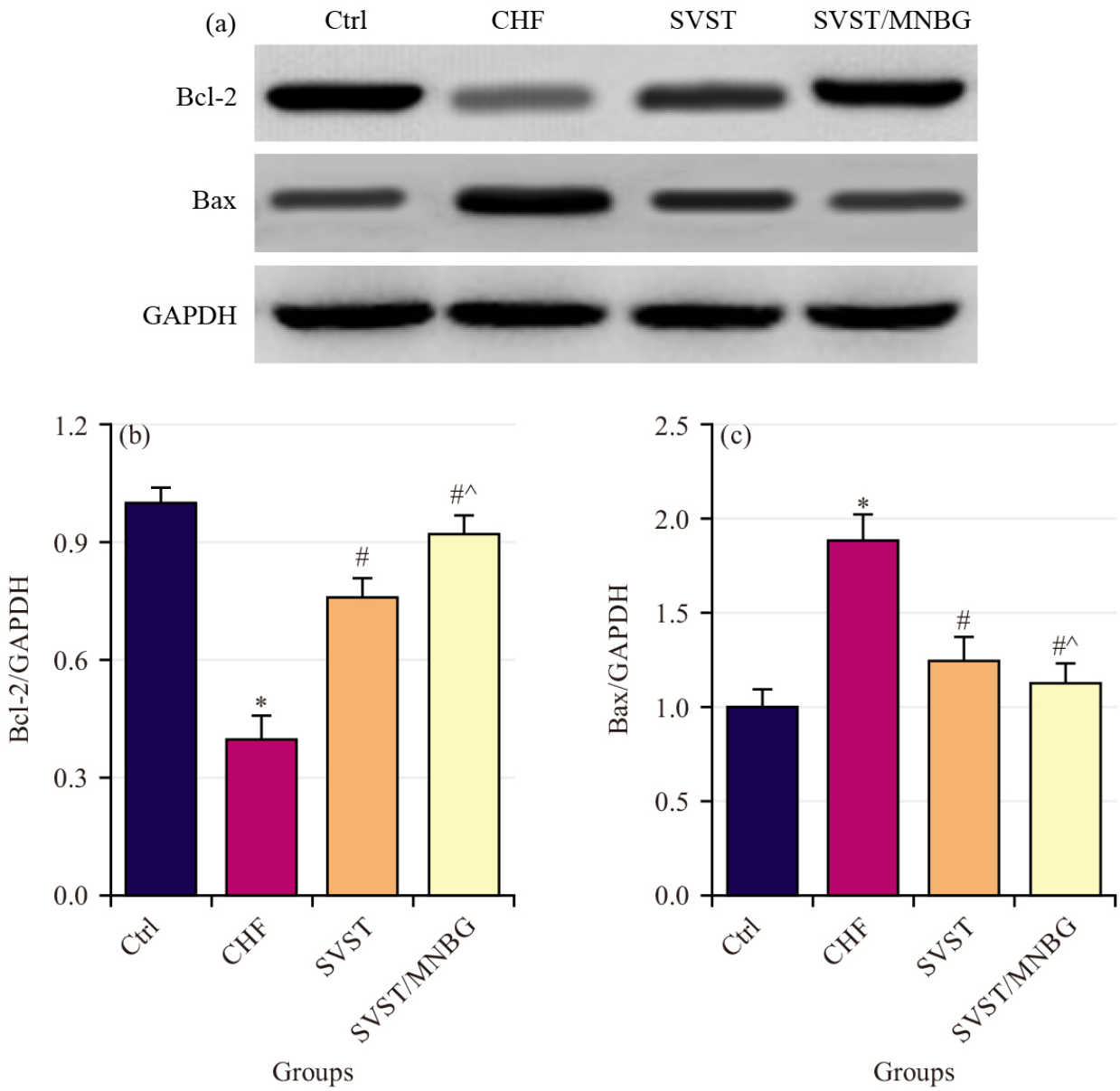

Fig. 5. Apoptosisrelated protein expression level in rat myocardial tissue. (a) Western blot detection result, (b) Relative expression level of Bcl-2 (Bcell lymphoma 2) and (c) Relative expression level of Bax. $*p < 0.05$ vs Ctrl group, $^{\#}p < 0.05$ vs CHF group and $^{\wedge}p < 0.05$ vs SVST group.

tivity, targeted delivery to diseased sites and controllable and sustained drug release [16,17]. Domingues *et al*. [18] reported that non-mesoporous BGs have a loading capacity for tetracycline drugs of less than 10%. In contrast, SVST/MNBG increased the loading capacity for SVST to approximately 33%, indicating a higher loading efficiency. Drug burst release occurs due to weak interactions between drug molecules and the material, causing rapid dissociation of the drug molecules [19]. The SVST/MNBG exhibited burst release of SVST within the first 0–12 hrs, but showed minimal fluctuations in drug release concentration from 24–504 hrs, indicating a controlled release mechanism for SVST.

The CHF represents the end stage of cardiovascular disease progression, with myocardial fibrosis and inflammation driven by comorbidities serving as crucial pathological foundations for CHF [20]. Reduced NO bioavailability leads to decreased binding with guanylate cyclase, resulting in lower levels of cyclic GMP and subsequently contributing to myocardial stiffness and hypertrophy [21,22]. The CK-MB, a marker widely present in myocardial tissue, is utilized to assess myocardial injury [23]. The NT-proBNP, a metabolic product of BNP, reflects the extent of myocardial damage [24]. In CHF rats, elevated expression levels of ROS, CK-MB and NT-proBNP, along with reduced NO, indicate observable myocardial damage. Croteau *et al*. [25]

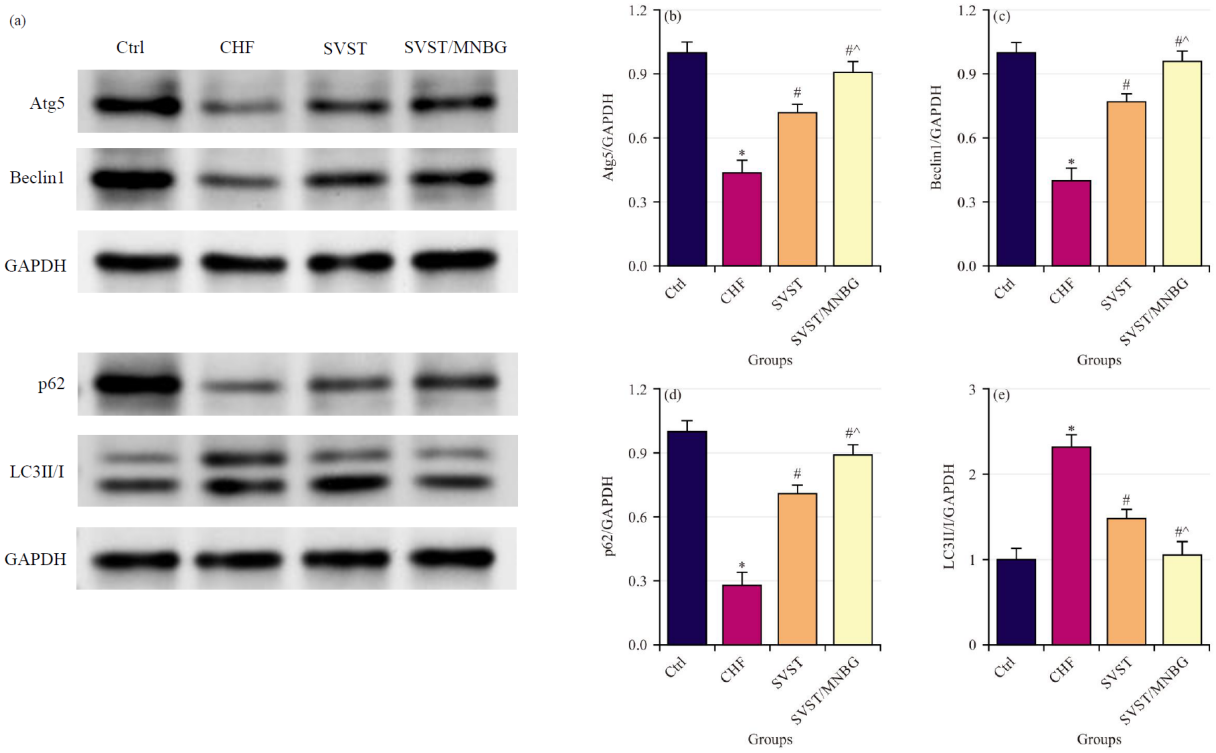

Fig. 6. Autophagyrelated protein expression level in rat myocardial tissue. (a) Western blot detection result, (b) Relative expression level of Atg5, (c) Relative expression level of Beclin1, (d) Relative expression level of p62 and (e) Relative expression level of LC3II/I. *$p < 0.05$ vs Ctrl group, $^{\#}p < 0.05$ vs CHF group and $^{\wedge}p < 0.05$ vs SVST group.

demonstrated that SVST can mitigate ROS accumulation in myocardial tissue and improve myocardial cell apoptosis in CHF rats. Similarly, the results findings showed that treatment with SVST and SVST/MNBG led to decreased ROS, CK-MB and NT-proBNP and increased NO in the myocardial tissue of CHF rats, with SVST/MNBG exhibiting superior effects on ROS and NO expression. These results suggested that SVST improved the oxidative stress state in CHF, thereby reducing the extent of myocardial damage associated with the condition.

The CHF is a multifactorial and complex cardiovascular disease characterized primarily by low cardiac output, myocardial alterations, cardiovascular dysfunction, metabolic abnormalities and neuroendocrine system disturbances [26]. Apoptosis of myocardial cells is one of the significant triggers of CHF. As myocardial cells undergo apoptosis, cardiac function progressively deteriorates, ultimately leading to the onset of CHF [27,28]. The Bcl-2 is known for its potent anti-apoptotic effects; it protects cells from apoptosis by inhibiting the activity of apoptosis-related factor Cyt C and the activation of the Caspase family [29]. The Bax undergoes conformational activation and translocation upon cellular stress, transforming into an oligomeric form that permeates the mitochondrial membrane. This process leads to the release of apoptosis-related factors into the cytosol and initiates the apoptosis cascade [30]. In CHF rat myocardial tissue, a decline in Bcl-2 protein expression level and an elevation in Bax protein expression level have been observed, indicating great myocardial cell apoptosis. Consequently, blocking myocardial cell apoptosis has emerged as a novel approach for CHF treatment. Subsequent findings revealed that administration of SVST and SVST/MNBG resulted in elevated Bcl-2 protein expression levels and reduced Bax protein expression levels in the myocardial tissue of CHF rats, with SVST/MNBG demonstrating a more pronounced effect on the expression of apoptosis-related proteins. The Atg5, a member of the autophagy-related protein family, is involved in regulating autophagosome formation and the degradation of intracellular waste materials [31]. The Beclin1, an initiator of autophagy, when upregulated, leads to cardiac dysfunction and promotes myocardial cell autophagy. The Beclin1 is positively correlated with myocardial cell autophagy and ventricular remodeling, making it a critical factor in the worsening of cardiac function in CHF [32,33]. The LC3 is a widely utilized marker for autophagosomes; LC3I can be converted to LC3II, which can serve as an indicator of autophagic activity [34]. The p62 is a substrate of LC3II and can regulate selective autophagic degradation through direct binding with LC3 [35]. In CHF rats, decreased expression levels of Atg5, Beclin1 and p62, along with increased LC3II/I ratios, indicate notable autophagy activation in myocardial tissue. Following administration of SVST and SVST/MNBG, expression lev-

els of Atg5, Beclin1 and p62 increased, while LC3II/I protein expression level decreased, with SVST/MNBG showing a more pronounced effect on autophagy-related protein expression. These results are consistent with the study by Zhai *et al.* [36], which demonstrated that inhibition of autophagy leads to cardiomyocyte senescence, thereby promoting cardiac dysfunction. This suggested that SVST can enhance cardiac function in CHF by inhibiting myocardial cell autophagy-apoptosis and MNBG improves the bioavailability of SVST, thereby enhancing its therapeutic efficacy.

5. Conclusion

Based on the results, a preliminary evaluation of the potential adoption of drug-loaded MNBG in treating CHF was conducted. The SVST/MNBG demonstrated a positive impact on CHF, indicating its potential efficacy as a therapeutic agent for HF. This effect may be attributed to its ability to mitigate myocardial damage, enhance myocardial contractility and modulate the autophagy-apoptosis pathways in myocardial cells. In summary, drug-loaded MNBG holds significant promise as a therapeutic modality in HF treatment. Nevertheless, further research is needed to elucidate the mechanisms of action, assess safety and efficacy and validate its feasibility and effectiveness in clinical applications.

6. Significance Statement

This study discovered the loading of sacubitril/valsartan tablets (SVST) onto mesoporous nanobioactive glass (MNBG) can be beneficial for the improvement of cardiac function in a chronic heart failure (CHF) model by modulating autophagy and apoptosis in cardiomyocytes. This innovative strategy demonstrates the enormous potential of SVST in enhancing the effects of CHF and offers new insights into precision medicine. It provides theoretical support for improving the efficacy of CHF treatment and contributes to a deeper understanding of the key mechanisms underlying the interaction between autophagy and apoptosis in the pathology of CHF; an area that has been insufficiently addressed in previous research. Thus, a new theory on optimizing related therapeutic approaches may be arrived at.

Availability of Data and Materials

The datasets used and analyzed during the current study are available from the corresponding author upon reasonable request.

Author Contributions

FJ and LL designed the research study. FJ, YM, XBG and LL performed the research. FJ and LL analyzed the data. FJ and LL drafted, proofread and revised the manuscript. All authors contributed to editorial changes in the manuscript. All authors read and approved the final manuscript. All authors have participated sufficiently in the work and agreed to be accountable for all aspects of the work.

Ethics Approval and Consent to Participate

All animal procedures were performed follow in the 3R principles and approved by the Ethics Committee of Tangshan Workers' Hospital (2022-KYLN-024).

Acknowledgment

Not applicable.

Funding

This research received no external funding.

Conflict of Interest

The authors declare no conflict of interest.

References

[1] Roger VL. Epidemiology of Heart Failure: A Contemporary Perspective. Circulation Research. 2021; 128: 1421–1434. https://doi.org/10.1161/CIRCRESAHA.121.318172.

[2] Seferović PM, Vardas P, Jankowska EA, Maggioni AP, Timmis A, Milinković I, *et al*. The Heart Failure Association Atlas: Heart Failure Epidemiology and Management Statistics 2019. European Journal of Heart Failure. 2021; 23: 906–914. https://doi.org/10.1002/ejhf.2143.

[3] Gao G, Chen W, Yan M, Liu J, Luo H, Wang C, *et al*. Rapamycin regulates the balance between cardiomyocyte apoptosis and autophagy in chronic heart failure by inhibiting mTOR signaling. International Journal of Molecular Medicine. 2020; 45: 195–209. https://doi.org/10.3892/ijmm.2019.4407.

[4] Liu Y, Fan D. Ginsenoside Rg5 induces G2/M phase arrest, apoptosis and autophagy via regulating ROS-mediated MAPK pathways against human gastric cancer. Biochemical Pharmacology. 2019; 168: 285–304. https://doi.org/10.1016/j.bcp.2019.07.008.

[5] Chen C, Wu X, Li Y, Peng Y. Study on the application effect of bisoprolol combined with sacubitril valsartan sodium tablets in the cardiac rehabilitation of patients with acute myocardial infarction combined with left heart failure after percutaneous coronary intervention (PCI). Annals of Palliative Medicine. 2021; 10: 5455–5461. https://doi.org/10.21037/apm-21-877.

[6] Liu Z, Wang J, Li Y. Efficacy of sacubitril valsartan sodium tablet for the treatment of chronic heart failure: A systematic review protocol of randomized controlled trials. Medicine. 2019; 98: e18050. https://doi.org/10.1097/MD.0000000000018050.

[7] Lin WY, Shao YJ, Chiang AF, Huang CC, Chiang KF, Chan CS, et al. Long-Term Outcomes of Sacubitril/Valsartan in Heart Failure with Reduced Ejection Fraction and Coexisting End-Stage Renal Disease. Clinical Pharmacology & Therapeutics. 2024; 116: 471–477. https://doi.org/10.1002/cpt.3315.

[8] Ye F, Li H, Chen X, Wang Y, Lin W, Chen H, *et al*. Efficacy and safety of sacubitril valsartan in treating heart failure with midrange ejection fraction after acute myocardial infarction in diabetic patients. Medicine. 2022; 101: e28729. https://doi.org/10.1097/MD.0000000000028729.

[9] Skallevold HE, Rokaya D, Khurshid Z, Zafar MS. Bioactive Glass Applications in Dentistry. International Journal of Molec-

ular Sciences. 2019; 20: 5960. https://doi.org/10.3390/ijms20235960.

[10] Syvänen J, Serlo W, Jalkanen J, Kohonen I, Raitio A, Nietosvaara Y, *et al*. Allograft Versus Bioactive Glass (BG-S53P4) in Pediatric Benign Bone Lesions: A Randomized Clinical Trial. The Journal of Bone and Joint Surgery. American Volume. 2023; 105: 659–666. https://doi.org/10.2106/JBJS.22.00716.

[11] Zeimaran E, Pourshahrestani S, Fathi A, Razak NABA, Kadri NA, Sheikhi A, *et al*. Advances in bioactive glass-containing injectable hydrogel biomaterials for tissue regeneration. Acta Biomaterialia. 2021; 136: 1–36. https://doi.org/10.1016/j.actbio.2021.09.034.

[12] Shi M, Zhao F, Sun L, Tang F, Gao W, Xie W, *et al*. Bioactive glass activates VEGF paracrine signaling of cardiomyocytes to promote cardiac angiogenesis. Materials Science & Engineering. C, Materials for Biological Applications. 2021; 124: 112077. https://doi.org/10.1016/j.msec.2021.112077.

[13] Clément S, Mehdi A. Sol-Gel Chemistry: From Molecule to Functional Materials. Molecules (Basel, Switzerland). 2020; 25: 2538. https://doi.org/10.3390/molecules25112538.

[14] Li H, Huang J, Liu C, Zhang Z, Song K, Ma K, *et al*. A New Model of Heart Failure Post-Myocardial Infarction in the Rat. Jove-Journal of Visualized Experiments. 2021; 172: e62540. https://doi.org/10.3791/62540.

[15] Kollias NS, Hess WJ, Johnson CL, Murphy M, Golab G. A literature review on current practices, knowledge, and viewpoints on pentobarbital euthanasia performed by veterinarians and animal remains disposal in the United States. Journal of the American Veterinary Medical Association. 2023; 261: 733–738. https://doi.org/10.2460/javma.22.08.0373.

[16] Malik JA, Ansari JA, Ahmed S, Khan A, Ahemad N, Anwar S. Nano-drug delivery system: a promising approach against breast cancer. Therapeutic Delivery. 2023; 14: 357–381. https://doi.org/10.4155/tde-2023-0020.

[17] Aggarwal N, Sachin, Nabi B, Aggarwal S, Baboota S, Ali J. Nano-based drug delivery system: a smart alternative towards eradication of viral sanctuaries in management of NeuroAIDS. Drug Delivery and Translational Research. 2022; 12: 27–48. https://doi.org/10.1007/s13346-021-00907-8.

[18] Domingues ZR, Cortés ME, Gomes TA, Diniz HF, Freitas CS, Gomes JB, *et al*. Bioactive glass as a drug delivery system of tetracycline and tetracycline associated with beta-cyclodextrin. Biomaterials. 2004; 25: 327–333. https://doi.org/10.1016/s0142-9612(03)00524-6.

[19] Cao C, Xue XR, Li QY, Zhang MJ, Abrahams BF, Lang JP. Phase Transition-Promoted Rapid Photomechanical Motions of Single Crystals of a Triene Coordination Polymer. Angewandte Chemie (International Ed. in English). 2023; 62: e202306048. https://doi.org/10.1002/anie.202306048.

[20] McLellan MA, Skelly DA, Dona MSI, Squiers GT, Farrugia GE, Gaynor TL, *et al*. High-Resolution Transcriptomic Profiling of the Heart During Chronic Stress Reveals Cellular Drivers of Cardiac Fibrosis and Hypertrophy. Circulation. 2020; 142: 1448–1463. https://doi.org/10.1161/CIRCULATIONAHA.119.045115.

[21] Vijay K, Neuen BL, Lerma EV. Heart Failure in Patients with Diabetes and Chronic Kidney Disease: Challenges and Opportunities. Cardiorenal Medicine. 2022; 12: 1–10. https://doi.org/10.1159/000520909.

[22] Hersberger L, Dietz A, Bürgler H, Bargetzi A, Bargetzi L, Kägi-Braun N, *et al*. Individualized Nutritional Support for Hospitalized Patients With Chronic Heart Failure. Journal of the American College of Cardiology. 2021; 77: 2307–2319. https://doi.org/10.1016/j.jacc.2021.03.232.

[23] Wei W, Zhang L, Zhang Y, Tang R, Zhao M, Huang Z, *et al*. Predictive value of creatine kinase MB for contrast-induced acute kidney injury among myocardial infarction patients. BMC Cardiovasc Disord. 2021; 21: 337. https://doi.org/10.1186/s12872-021-02155-7.

[24] Rørth R, Jhund PS, Yilmaz MB, Kristensen SL, Welsh P, Desai AS, *et al*. Comparison of BNP and NT-proBNP in Patients With Heart Failure and Reduced Ejection Fraction. Circulation. Heart Failure. 2020; 13: e006541. https://doi.org/10.1161/CIRCHEARTFAILURE.119.006541.

[25] Croteau D, Qin F, Chambers JM, Kallick E, Luptak I, Panagia M, *et al*. Differential Effects of Sacubitril/Valsartan on Diastolic Function in Mice With Obesity-Related Metabolic Heart Disease. JACC. Basic to Translational Science. 2020; 5: 916–927. https://doi.org/10.1016/j.jacbts.2020.07.006.

[26] Heidenreich PA, Bozkurt B, Aguilar D, Allen LA, Byun JJ, Colvin MM, *et al*. 2022 AHA/ACC/HFSA Guideline for the Management of Heart Failure: A Report of the American College of Cardiology/American Heart Association Joint Committee on Clinical Practice Guidelines. Circulation. 2022; 145: e895–e1032. https://doi.org/10.1161/CIR.0000000000001063.

[27] Mascolo A, di Mauro G, Cappetta D, De Angelis A, Torella D, Urbanek K, *et al*. Current and future therapeutic perspective in chronic heart failure. Pharmacological Research. 2022; 175: 106035. https://doi.org/10.1016/j.phrs.2021.106035.

[28] Wei W, Qingling LI, Qiang MA, Ran X, Bing G, Yi W, *et al*. Effects of moxibustion at bilateral Feishu (BL13) and Xinshu (BL15) combined with benazepril on myocardial cells apoptosis index and apoptosis-related proteins cytochrome c and apoptosis-inducing factor in rats with chronic heart failure. Journal of Traditional Chinese Medicine = Chung i Tsa Chih Ying Wen Pan. 2022; 42: 227–233. https://doi.org/10.19852/j.cnki.jtcm.20220126.001.

[29] Hao Q, Chen J, Lu H, Zhou X. The ARTS of p53-dependent mitochondrial apoptosis. Journal of Molecular Cell Biology. 2023; 14: mjac074. https://doi.org/10.1093/jmcb/mjac074.

[30] Quarato G, Mari L, Barrows NJ, Yang M, Ruehl S, Chen MJ, *et al*. Mitophagy restricts BAX/BAK-independent, Parkin-mediated apoptosis. Science Advances. 2023; 9: eadg8156. https://doi.org/10.1126/sciadv.adg8156.

[31] Baeva ME, Camara-Lemarroy C. The role of autophagy protein Atg5 in multiple sclerosis. Multiple Sclerosis and Related Disorders. 2023; 79: 105029. https://doi.org/10.1016/j.msard.2023.105029.

[32] Hebah HA, Kamel HM, Bastawy IM, Ahmed FA. Association between serum beclin 1 level and cardiac valvular calcification in hemodialysis patients. Current Problems in Cardiology. 2024; 49: 102519. https://doi.org/10.1016/j.cpcardiol.2024.102519.

[33] Chai Q, Zhang W, Gao L, Yang Y, Miao M, Liu D, *et al*. The Action and Mechanism of Trehalose on GATA4 Autophagy Degradation and Ventricular Remodeling. Discovery Medicine. 2023; 35: 394–404. https://doi.org/10.24976/Discov.Med.202335176.40.

[34] Peña-Martinez C, Rickman AD, Heckmann BL. Beyond autophagy: LC3-associated phagocytosis and endocytosis. Science Advances. 2022; 8: eabn1702. https://doi.org/10.1126/sciadv.abn1702.

[35] Jeong SJ, Zhang X, Rodriguez-Velez A, Evans TD, Razani B. p62/*SQSTM1* and Selective Autophagy in Cardiometabolic Diseases. Antioxidants & Redox Signaling. 2019; 31: 458–471. https://doi.org/10.1089/ars.2018.7649.

[36] Zhai P, Sung EA, Shiheido-Watanabe Y, Takayama K, Tian Y, Sadoshima J. Suppression of autophagy induces senescence in the heart. Journal Molecular and Cellular Cardiology. 2024; 195: 83-96. https://doi.org/10.1016/j.yjmcc.2024.08.001.